Effects of Viscosity Variations on Buoyancy-Driven Flow from a Horizontal Circular Cylinder Immersed in Al_2O_3-Water Nanofluid

Habibi, Mohammad Reza; Amini, Meysam*+

Energy Technologies Research Division, Research Institute of Petroleum Industry (RIPI), Tehran, I.R. IRAN

Arefmanesh, Aref

Department of Mechanical Engineering, University of Kashan, Kashan, I.R. IRAN

Ghasemikafrudi, Esmaeil

Energy Technologies Research Division, Research Institute of Petroleum Industry (RIPI), Tehran, I.R. IRAN

ABSTRACT: *The buoyancy-driven boundary-layer flow from a heated horizontal circular cylinder immersed in a water-based alumina (Al_2O_3) nanofluid is investigated using variable properties for nanofluid viscosity. Two different viscosity models are utilized to evaluate heat transfer enhancement from a cylinder. Exact analytic solutions of the problem are attained employing a novel powerful technique is known as the Optimal Homotopy Analysis Method (OHAM). The accuracy and reliability of the results are verified by comparing them with experimental results in the literature. It is found that the characteristics of flow and temperature distributions are significantly influenced by the volume fraction of alumina nanoparticles, as well as nanofluid viscosity models. Enhancing the volume fraction of nanoparticles, the surface shear stress and the local Nusselt number both increase in the middle regions of the cylinder. The results also indicated that with increasing the nanoparticles volume fraction, isotherms become less dense and the absolute values of the stream-function decrease within the domain. Based on the results of the parametric study, two correlations (based on two different effective viscosity models) are proposed for the average Nusselt number of the alumina-water nanofluid in terms of volume fraction of the nanoparticles and the Rayleigh number which can be used as benchmarks for future investigations. However, uncertainties of viscosity models showed different manners on heat transfer coefficient versus nanoparticles volume fraction.*

EYWORDS: *Natural convection; Nanofluid; Horizontal cylinder; Analytical solution; Viscosity models.*

INTRODUCTION

The Buoyancy-driven flow of an incompressible viscous fluid about a horizontal circular-shape cylinder represents a notable problem which has been substantially investigated experimentally and numerically because

***** *To whom correspondence should be addressed.*

+ E-mail: aminime@ripi.ir

1021-9986/2019/1/213- 20/$/7.00

of its engineering applications which include heaters, refrigerators, vaporizers, heat exchangers, hot water and steam pipes, air cooling systems for air conditioning, electrical conductors, and passive solar heating.

In 1976, *Sparrow* and *Lee* [1] examined the problem of a vertical stream over a heated horizontal cylinder with circular cross-section for mixed convection. *Merkin* [2-4] was the first investigator who completely solved this problem by employing the methods of Blasius and Görtler series expansion along with a finite difference scheme and an integral method. *Ingham* [5] also investigated the convective boundary-layer flow and heat transfer along an isothermal horizontal cylinder. *Kuehn* and *Goldstein* [6] studied the laminar buoyancy-driven flow of air from an isothermal cylinder utilizing a numerical procedure. Their results were obtained for different values of Rayleigh numbers. *Merkin* and *Pop* [7] analyzed the natural convection boundary layer flow on an isoflux horizontal circular cylinder. In 1997, *Morgan* [8] conducted an extensive review of many theoretical, numerical and experimental studies on overall natural convective heat transfer from horizontal cylinders for Prandtl, Pr, equal to 0.7, and for Rayleigh numbers from 10 to 10^7. He concluded that, due to the dispersions in the results, there were still uncertainties about the values of the mean Nusselt number, *Nu*. *Nazar et al.* [9] numerically solved the problem of free convection of micropolar fluid flow along an isoflux horizontal circular cylinder. *Molla et al.* investigated the effects of temperature dependent viscosity [10], heat generation [11], and wall heat flux [12] on free convection boundary-layer flow from a horizontal cylinder, numerically, conducting implicit finite difference method together with the Keller-box scheme. In order to explore the effects of the angular position and the cylinder diameter on the local heat transfer, *Chung et al.* [13] investigated free convection flow and heat transfer phenomena on horizontal cylinders experimentally. *Prhashanna* and *Chhabra* [14] studied the laminar natural convection boundary layer flow and heat transfer from a horizontal circular cylinder submerged in quiescent power-law fluids, numerically. They observed that the local heat transfer coefficient declines from its maximum value at the front impingement point along the circumference of the cylinder. *Azim* and *Chowdhury* [15] analyzed the effects of heat generation and Joule heating on MHD-conjugate free convection over a horizontal circular cylinder numerically using Keller box method. A similar research work is also carried out by *Bhuiyan et al.* [16] which they have taken into account the effects of viscous dissipation, as well as Joule heating and magnetic field on free convection heat transfer from a horizontal cylinder. *Javed et al.* [17] investigated the natural convection boundary-layer flow around a horizontal circular cylinder under the effects of magnetic field and radiation. *Sebastian* and *Shine* [18] studied the buoyancy-driven flow along a circular cylinder with and without confinement numerically, using finite volume approach. They presented the heat transfer results for a wide range of the Rayleigh number. It should be noted that none of the above mentioned research works came up with an exact analytic solution to the problem of natural convection along a horizontal circular cylinder regardless the working fluid media.

The low thermal conductivity of a conventional fluid such as air or water is the main drawback against the heat transfer enhancement in the free convection heat transfer regimes. A nanofluid, a suspension of nano-sized particles in a base fluid, possesses a higher thermal conductivity compared to that of the base fluid, and, therefore, is expected to surpass the heat transfer performance. A comprehensive survey of the works related to the nanofluids and their heat transfer characteristics can be found in a book by *Das et al*. [19], in a number of recent review papers [20-22], and in several recent research works [23-38].

There are very few recent studies dealing with convective heat transfer along bodies immersed in a nanofluid medium. *Valipour* and *Ghadi* [39] investigated the flow distribution and force convection heat transfer through a Cu-water nanofluid around a circular cylinder numerically using a finite volume method. They estimated the effective viscosity and the effective thermal conductivity of nanofluid by Brinkman and Hamilton-Crosser models, respectively, and came up with that fact that the local and mean Nusselt numbers are enhanced as a result of adding nanoparticles to the base fluid. *Nazar et al.* [40] studied the steady mixed convection flow and heat transfer over an isothermal horizontal cylinder embedded in a nanofluid-filled porous medium for both cases of heated and cooled cylinders numerically, employing an implicit finite-difference scheme. *Tham et al.* [41] carried out similar work to the one conducted by *Nazar et al.* [40]

considering the effects of nanofluid thermophoresis and Brownian motion. *Prasad et al.* [42] and [43] conducted a numerical approach to the problem of natural convection heat and mass transfer of a nanofluid along a horizontal cylinder considering non-Newtonian and micropolar fluids as the working fluid. They reported their results based on the effects of thermophoresis and Brownian motion of the nanofluid. In a similar study, the effects of thermophoresis and Brownian motion on heat and mass transfer of a nanofluid flow along a circular cylinder embedded in porous media is numerically investigated by *Reddy* and *Chamkha* [44] using a validated Finite element method.

The above literature review reveals that neither a comprehensive analysis nor an exact analytic solution exists for the problem of buoyancy-driven flow of a nanofluid along a horizontal heated circular cylinder considering the viscosity uncertainties. It is to be noted that in the all of the previous research works, an exact solution for the governing differential equations was found to be inaccessible due to the non-linearity in the Navier–Stokes equations and/or the boundary conditions. Among the various analytical methods, homotopy method is one of the most powerful and superior techniques which provide the possibility to solve a set of coupled partial differential equations while offers great advantage of high flexibility to achieve reliable series solutions [45].

In the present study, the Optimal Homotopy Analysis Method (OHAM) is extended to the case of natural convection boundary-layer flow and heat transfer from an isothermal heated circular cylinder immersed in a cold nanofluid. Al_2O_3-water nanofluid is considered as the working medium. Two different viscosity models, namely, the *Brinkman* [46] formula and the correlation proposed by *Maïga et al.* [47] are employed for the effective viscosity of the nanofluid. Using the OHAM, closed-form solutions are obtained for the velocity and temperature fields. Subsequently, a parametric study is performed, and the effects of the nanoparticles volume fraction on the velocity and temperature fields are investigated. Finally, correlations are proposed for the average Nusselt number of Al_2O_3-water nanofluid in terms of the diametrical-based Rayleigh number and the nanoparticles volume fraction.

GOVERNING EQUATIONS

A steady, laminar, two-dimensional natural convective flow from a horizontal circular cylinder of radius *a*, immersed in a viscous incompressible Al_2O_3-water nanofluid is considered (Fig. 1). The $\hat{x}$ and $\hat{y}$ are coordinates measured perpendicular and along to the surface of the cylinder, respectively, with an origin at the lower stagnation point ($\hat{y} \approx 0$). The cylinder and the surrounding nanofluid are maintained at differentially-different constant temperatures of T_w and T_∞, respectively, with $T_w > T_\infty$. The 2D physical representation of the cylinder and the coordinate system are shown in Fig.1.

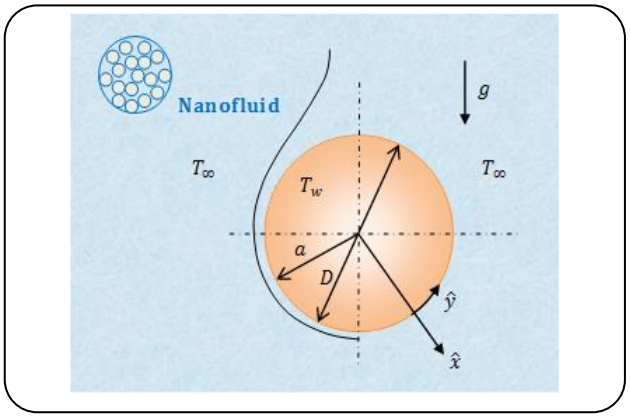

Fig. 1: Physical configuration and the local coordinate system.

Employing the boundary layer and the Boussinesq approximations, the equations for conservations of mass, momentum, and energy can be derived as the following form:

$$\frac{\partial \hat{u}}{\partial \hat{x}} + \frac{\partial \hat{v}}{\partial \hat{y}} = 0 \tag{1}$$

$$\hat{u}\frac{\partial \hat{v}}{\partial \hat{x}} + \hat{v}\frac{\partial \hat{v}}{\partial \hat{y}} = \frac{1}{\rho_{nf}}\left[\mu_{nf}\frac{\partial^2 \hat{v}}{\partial \hat{x}^2} + (\rho\beta)_{nf}\, g(T - T_\infty)\sin\left(\frac{\hat{y}}{a}\right)\right] \tag{2}$$

$$\hat{u}\frac{\partial T}{\partial \hat{x}} + \hat{v}\frac{\partial T}{\partial \hat{y}} = \alpha_{nf}\frac{\partial^2 T}{\partial \hat{x}^2} \tag{3}$$

Where $(\hat{u}, \hat{v})$ are the velocity components along the $(\hat{x}, \hat{y})$ axes, and the kinematic viscosity, υ_{nf}, the thermal expansion coefficient, β_{nf}, and the thermal diffusivity, α_{nf}, of the nanofluid are constants values evaluated at the temperature $T = T_\infty$. The respective boundary conditions for Eqs. (1) – (3) are

$$\hat{u} = \hat{v} = 0, \quad T = T_w \quad \text{at} \quad \hat{x} = 0 \tag{4}$$

$$\hat{v} \to 0, \quad T \to T_\infty \quad \text{at} \quad \hat{x} \to \infty \tag{5}$$

To convert the governing equations into a non-dimensional form, the dimensionless variables are introduced as follows:

$$x = \left(Ra_a\right)^{\frac{1}{4}}\left(\frac{\hat{x}}{a}\right), \quad y = \frac{\hat{y}}{a}, \quad \theta = \frac{T - T_\infty}{T_w - T_\infty} \tag{6}$$

$$u = \frac{a}{a_f}\left(Ra_a\right)^{\frac{1}{4}}\hat{u}, \quad v = \frac{a}{a_f}\left(Ra_a\right)^{-\frac{1}{2}}\hat{v}$$

where Ra_a is the Rayleigh number based on the radius of the cylinder which is defined as

$$Ra_a = g\beta_f\left(T_w - T_\infty\right)\frac{a^3}{\nu_f a_f} \tag{7}$$

Inserting the above dimensionless variables into Eqs. (1) – (3) lead to the following non-dimensional equations:

$$\frac{\partial u}{\partial x} + \frac{\partial v}{\partial y} = 0 \tag{8}$$

$$\frac{1}{Pr}\left(u\frac{\partial v}{\partial x} + v\frac{\partial v}{\partial y}\right) = A_1\frac{\partial^2 v}{\partial x^2} + A_2\theta\sin y \tag{9}$$

$$u\frac{\partial \theta}{\partial x} + v\frac{\partial \theta}{\partial y} = A_3\frac{\partial^2 v}{\partial x^2} \tag{10}$$

where

$$A_1 = \frac{\nu_{nf}}{\nu_{nf}}, \quad A_2 = \frac{(\rho\beta)_{nf}}{(\rho\beta)_f}\frac{\rho_f}{\rho_{nf}}, \quad A_3 = \frac{\alpha_{nf}}{\alpha_f} \tag{11}$$

The corresponding dimensionless forms of the boundary conditions are

$$u = v = 0, \quad \theta = 1 \quad \text{at} \quad x = 0 \tag{12}$$

$$v \to 0, \quad \theta \to 1 \quad \text{as} \quad x \to \infty \tag{13}$$

In order to solve Eqs. (8) – (9), subject to the above boundary conditions, the following non-similar transformations are introduced:

$$\psi = yf\left(x, y\right) \quad \text{and} \quad \theta = \theta\left(x, y\right) \tag{14}$$

where the stream function, ψ, can be defined as

$$u = \frac{\partial \psi}{\partial y} \quad \text{and} \quad v = -\frac{\partial \psi}{\partial x} \tag{15}$$

Substituting (13) – (14) into Eqs. (8) – (10) yields the following transformed equations after some algebraic manipulations:

$$\frac{1}{Pr}\left[\left(\frac{\partial f}{\partial x}\right)^2 - f\frac{\partial^2 f}{\partial x^2} + y\left(\frac{\partial f}{\partial x}\frac{\partial^2 f}{\partial x \partial y} - \frac{\partial f}{\partial y}\frac{\partial^2 f}{\partial x^2}\right)\right] \tag{16}$$

$$f\frac{\partial \theta}{\partial x} + y\left(\frac{\partial f}{\partial x}\frac{\partial \theta}{\partial y} - \frac{\partial \theta}{\partial x}\frac{\partial f}{\partial y}\right) = A_3\frac{\partial^2 \theta}{\partial x^2} \tag{17}$$

The transformed boundary conditions correspond to the above equations are

$$f = \frac{\partial f}{\partial x} = 0 \quad \theta = 1 \quad \text{at} \quad x = 0 \tag{18}$$

$$\frac{\partial f}{\partial x} \to 0 \quad \theta \to 0 \quad \text{as} \quad x \to \infty \tag{19}$$

Thermophysical Properties of the Nanofluid

As stated previously, Al_2O_3-water nanofluid is employed as the working fluid in the present study. The thermophysical properties of the base fluid (Pr = 6.2) and the nanoparticles are summarized in Table 1.

Various relations for the effective thermophysical properties of the nanofluids are available in the literature. The prominent empirical models on predicting the viscosity of nanofluids are presented in Table 2. Moreover, Fig. 2 shows a graphical comparison between these models.

In order to gain a better understanding of the nanofluid viscosity variations, two formulas for the viscosity of the nanofluid, namely, the Brinkman [46] formula and *Maïga et al.'s* correlation [47], here referred to as Model I and Model II, respectively, are considered in the current investigation. Actually, due to the variety of existing models (Fig. 2), and to cope with the admissible range of the above-mentioned empirical models, the former is considered as the lower bound, while the latter correlation is regarded as the upper/moderate bound of the nanofluid viscosity variations.

According to the Brinkman model (Model I), the following relation is proposed for the effective dynamic viscosity of a nanofluid

$$\mu_{eff} = \mu_f \big/ \left(1 - \phi\right)^{2.5} \tag{20}$$

Table 1: Thermophysical properties of the base fluid and the nanoparticles.

Physical property	Water	Al_2O_3-nanoparticles
ρ (kg m^{-3})	997.1	3970
c_p (J kg^{-1} K^{-1})	4179	765
k (W m^{-1} K^{-1})	0.613	40
$\beta \times 10^5$ (K^{-1})	21	0.85

Table 2: Summary of the most well-known empirical correlations for the effective viscosity of nanofluids.

Model	**Correlation**
Brinkman [46]	$\mu_{eff} = \mu_f / (1-\phi)^{2.5}$
Maïga et al. [47]	$\mu_{eff} = \mu_f \left(1+7.3\phi+123\phi^2\right)$
Batchelor [48]	$\mu_{eff} = \mu_f \left(1+2.5\phi+6.5\phi^2\right)$
Corcione [49]	$\mu_{nf} = \mu_f \left(1/1-34.87\left(d_p/d_f\right)^{-0.3} \phi^{1.03}\right)$
Heyhat et al. [50]	$\mu_{nf} = \mu_f \mathrm{Exp}\left(\frac{5.989\phi}{0.278-\phi}\right)$
Chandrasekar et al. [51]	$\mu_{nf} = \mu_f \left(1+5200\left(\frac{\phi}{1-\phi}\right)^{2.8}\right)$
Sekhar and Sharma [52]	$\mu_{nf} = 0.935\mu_f \left(1+T_{nf}/70\right)^{0.5605} \left(1+d_p/80\right)^{0.05915} \left(1+\phi/100\right)^{10.51}$
Hatschek [53]	$\mu_{eff} = \mu_f \left(1+4.5\phi\right)$

■ *Assuming: d_p = 50 nm, and $T_{nf} \approx T_{bulk}$ = 25°C.*

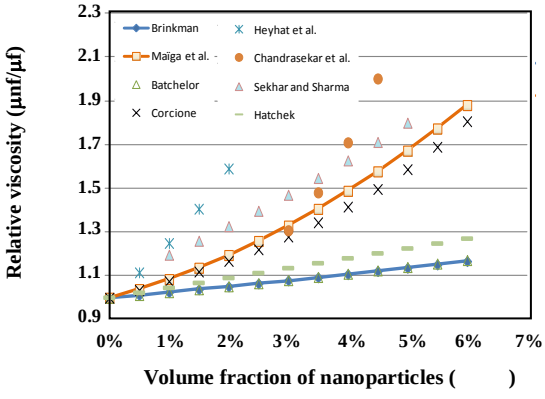

Fig. 2: Comparison between the nanofluid viscosity to that of the base fluid for prominent empirical models

where μ_f is the viscosity of the base fluid, and ϕ denotes the volume fraction of the nanoparticles. The *Maïga et al.*'s correlation (Model II) is expressed as

$$\mu_{eff} = \mu_f \left(1+7.3\phi+123\phi^2\right) \tag{21}$$

The density, ρ_{nf}, the heat capacity, $(\rho c_p)_{nf}$, and the thermal expansion coefficient, β_{nf} of the nanofluids can be obtained from the following respective equations:

$$\rho_{nf} = (1-\phi)\rho_f + \phi\rho_p \tag{22}$$

$$\left(\rho c_p\right)_{nf} = (1-\phi)\left(\rho c_p\right)_f + \phi\left(\rho c_p\right)_p$$

$$\beta_{nf} = \frac{(1-\phi)(\rho\beta)_f + \phi\left(\rho c_p\right)_p}{(1-\phi)\rho_f} + \phi\rho_f \tag{23}$$

The thermal diffusivity of the nanofluids, α_{nf}, is obtained from

$$\alpha_{nf} = k_{nf} / \left(\rho c_p\right)_{nf} \tag{24}$$

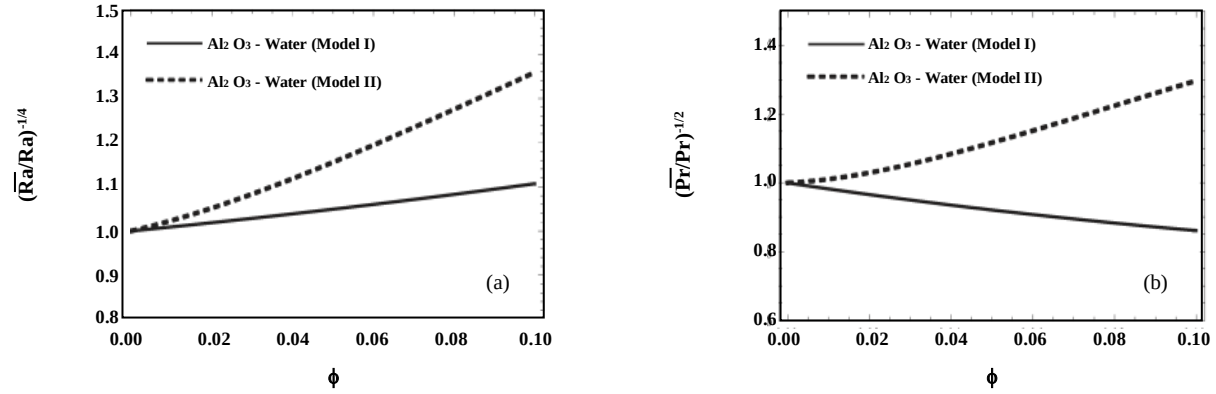

Fig. 3: Ratio of the Ra and Pr of the nanofluid to that of the base fluid: (a) Rayleigh numbers ratio; (b) Prandtl numbers ratio.

Where for spherical nanoparticles, the nanofluid effective thermal conductivity, k_{nf} can be evaluated from the Maxwell Garnett (MG) model [54]

$$k_{nf} = k_f \left[\frac{\left(k_p + 2k_f\right) - 2\phi\left(k_f - k_p\right)}{\left(k_p + 2k_f\right) + \phi\left(k_f - k_p\right)} \right] \tag{25}$$

Where k_f and k_p are the thermal conductivities of the base fluid and the nanoparticles, respectively. Considering the above relations for the thermophysical properties of the nanofluids and the definitions of the Rayleigh and Prandtl numbers for a nanofluid, the variations of $\left(\overline{Ra}_a / Ra_a\right)^{-1/4}$ and $\left(\overline{Pr}/Pr\right)^{1/2}$ with the volume fraction of the nanoparticles for the Al_2O_3-water nanofluid (Models I and II) are presented for future reference in Figs. 3(a) and (b), respectively.

The local Nusselt number of the nanofluids based on the radius of the horizontal cylinder is assessed as follows:

$$\left(Nu_a\right)_{nf} = \frac{h_{nf}\, a}{k_f} = \frac{q''_{w,a}}{\left(T_w - T_\infty\right)} \frac{a}{k_f} = \tag{26}$$

$$\frac{-k_{nf}\left(\frac{\partial T}{\partial \hat{x}}\right)_{\hat{x}=0}}{\left(T_w - T_\infty\right)} \frac{a}{k_f} = -\frac{k_{nf}}{k_f}\left(\frac{\partial \theta(x,y)}{\partial x}\right)_{x=0} Ra_a^{\frac{1}{4}}$$

The shear stress on the tube surface can be defined as:

$$\tau_w(x,y) = \mu_{nf}\left(\frac{\partial \hat{v}(\hat{x},\hat{y})}{\partial \hat{x}}\right)_{\hat{x}=0} \tag{27}$$

Which can be written in a non-dimensional form as

$$\frac{\tau_w(x,y)}{\alpha_f \mu_f\, Ra_a^{1/4}/a^2} = -\frac{\mu_{nf}}{\mu_f} y\left(\frac{\partial^2 f(x,y)}{\partial x^2}\right)_{x=0} \tag{28}$$

HAM SOLUTION

In order to solve Eqs. (16) and (17) by the HAM, the unknown functions $f(x,y,\phi)$ and $\theta(x,y,\phi)$ are written in terms of a set of base functions multiplied by unknown coefficients. To satisfy the far-field boundary conditions (Eqs. ((18) and (19)) unanimously, the following base functions are chosen:

$$\left\{ y^k \sin^p y \cos^q y \exp\left(-n\lambda x\right)\big|_n \geq 0, > \right. \tag{29}$$
$$\left. 0, p \geq 0, q \geq 0, k \geq 0 \quad \text{or} \quad = -1 \right\}$$

Where $\lambda > 0$ is a spatial-scale parameter. Hence, f and θ are expressed in the form of the following series:

$$f(x,y,\phi) = \tag{30}$$
$$\sum_{k=0}^{+\infty}\sum_{p=0}^{+\infty}\sum_{q=0}^{+\infty}\sum_{n=0}^{+\infty} a_{p,q,n}^k y^k \sin^p y \cos^q y \exp\left(-n\lambda x\right)$$

$$\theta(x,y,\phi) = \tag{31}$$
$$\sum_{k=0}^{+\infty}\sum_{p=0}^{+\infty}\sum_{q=0}^{+\infty}\sum_{n=0}^{+\infty} b_{p,q,n}^k y^k \sin^p y \cos^q y \exp\left(-n\lambda x\right)$$

Where $a_{p,q,n}^k$ and $b_{p,q,n}^k$ are unknown coefficients. Based on the above solution expressions, and considering the boundary conditions at the plate surface (Eq. (18)), the following initial approximations f_0 and θ_0 for f and θ are selected, respectively:

$$f_0(x,y) = -\frac{1}{\lambda}\left(1 - 2\exp\left(-\lambda x\right) + \exp\left(-2\lambda x\right)\right) \tag{32}$$

$$\theta_0(x,y) = \exp\left(-\lambda x\right) \tag{33}$$

The following auxiliary linear operators $\mathcal{L}_1$ and $\mathcal{L}_2$ acting on f and θ, respectively, are defined:

$$\mathcal{L}_1(\mathrm{f}) = \frac{\partial^3 \mathrm{f}}{\partial \mathrm{x}^3} + \lambda \frac{\partial^2 \mathrm{f}}{\partial \mathrm{x}^2} \tag{34}$$

$$\mathcal{L}_2(\theta) = \frac{\partial^2 \theta}{\partial \mathrm{x}^2} + \lambda \frac{\partial \theta}{\partial \mathrm{x}} \tag{35}$$

which satisfy the following conditions:

$$\mathcal{L}_1\left(\mathrm{C}_1 + \mathrm{C}_2 \exp(-\lambda \mathrm{x}) + \mathrm{C}_3 \mathrm{x}\right) = 0 \tag{36}$$

$$\mathcal{L}_2\left(\mathrm{C}_4 + \mathrm{C}_5 \exp(-\lambda \mathrm{x})\right) = 0 \tag{37}$$

irrespective of the values of coefficients C_i (i = 1,2,…,5). Considering Eqs. (15) and (16), the following non-linear operators are defined:

$$\mathrm{N}_1\left[\hat{\mathrm{f}}(\mathrm{x},\mathrm{y};\mathrm{q}), \hat{\theta}(\mathrm{x},\mathrm{y};\mathrm{q})\right] = \mathrm{A}_1 \frac{\partial^3 \hat{\mathrm{f}}(\mathrm{x},\mathrm{y};\mathrm{q})}{\partial \mathrm{x}^3} - \tag{38}$$
$$\mathrm{A}_2 \frac{\sin \mathrm{y}}{\mathrm{y}} \hat{\theta}(\mathrm{d},\mathrm{y};\mathrm{q}) + \frac{1}{\mathrm{pr}}\left[\left(\frac{\partial \hat{\mathrm{f}}(\mathrm{x},\mathrm{y};\mathrm{q})}{\partial \mathrm{x}}\right)^2 - \right.$$
$$\hat{\mathrm{f}}(\mathrm{x},\mathrm{y};\mathrm{q}) \frac{\partial^2 \hat{\mathrm{f}}(\mathrm{x},\mathrm{y};\mathrm{q})}{\partial \mathrm{x}^2} + \mathrm{y}\left(\frac{\partial \hat{\mathrm{f}}(\mathrm{x},\mathrm{y};\mathrm{q})}{\partial \mathrm{x}} \frac{\partial^2 \hat{\mathrm{f}}(\mathrm{x},\mathrm{y};\mathrm{q})}{\partial \mathrm{x} \partial \mathrm{y}} - \right.$$
$$\left.\left.\frac{\partial \hat{\mathrm{f}}(\mathrm{x},\mathrm{y};\mathrm{q})}{\partial \mathrm{y}} \frac{\partial^2 \hat{\mathrm{f}}(\mathrm{x},\mathrm{y};\mathrm{q})}{\partial \mathrm{x}^2}\right)\right]$$

$$\mathrm{N}_2\left[\hat{\mathrm{f}}(\mathrm{x},\mathrm{y};\mathrm{q}), \hat{\theta}(\mathrm{x},\mathrm{y};\mathrm{q})\right] = \mathrm{A}_3 \frac{\partial^2 \hat{\theta}(\mathrm{x},\mathrm{y};\mathrm{q})}{\partial \mathrm{x}^2} - \tag{39}$$
$$\hat{\mathrm{f}}(\mathrm{x},\mathrm{y};\mathrm{q}) \frac{\partial \hat{\theta}(\mathrm{x},\mathrm{y};\mathrm{q})}{\partial \mathrm{x}} - \mathrm{y}\left(\frac{\partial \hat{\mathrm{f}}(\mathrm{x},\mathrm{y};\mathrm{q})}{\partial \mathrm{x}} \frac{\partial \theta(\mathrm{x},\mathrm{y};\mathrm{q})}{\partial \mathrm{y}} - \right.$$
$$\left.\left.\frac{\partial \hat{\theta}(\mathrm{x},\mathrm{y};\mathrm{q})}{\partial \mathrm{y}} \frac{\partial \hat{\mathrm{f}}(\mathrm{x},\mathrm{y};\mathrm{q})}{\partial \mathrm{y}}\right)\right]$$

Where $q \in [0,1]$ is an embedding parameter, and $\hat{\mathrm{f}}(\mathrm{x},\mathrm{y};\mathrm{q})$ and $\hat{\theta}(\mathrm{x},\mathrm{y};\mathrm{q})$ are nonzero real functions of x, y, and q. Subsequently, the following *zeroth-order deformation equations* are constructed:

$$(1-\mathrm{q})\mathcal{L}_1\left(\hat{\mathrm{f}}(\mathrm{x},\mathrm{y};\mathrm{q}) - \mathrm{f}_0(\mathrm{x},\mathrm{y})\right) = \tag{40}$$
$$\mathrm{q}\hbar \mathrm{H}_\mathrm{f} \mathrm{N}_1\left[\hat{\mathrm{f}}(\mathrm{x},\mathrm{y};\mathrm{q}), \hat{\theta}(\mathrm{x},\mathrm{y};\mathrm{q})\right]$$

$$(1-\mathrm{q})\mathcal{L}_2\left(\hat{\theta}(\mathrm{x},\mathrm{y};\mathrm{q}) - \theta_0(\mathrm{x},\mathrm{y})\right) = \tag{41}$$
$$\mathrm{q}\hbar_\theta \mathrm{H}_\theta \mathrm{N}_2\left[\hat{\mathrm{f}}(\mathrm{x},\mathrm{y};\mathrm{q}), \hat{\theta}(\mathrm{x},\mathrm{y};\mathrm{q})\right]$$

Where $\hbar_f$ and $\hbar_\theta$ are nonzero auxiliary parameters, and H_f (η) and H_θ (η) are nonzero auxiliary functions. The boundary conditions for the above equations are:

$$\hat{\mathrm{f}}(0,\mathrm{y};\mathrm{q}) = 0 \quad \hat{\mathrm{f}}'(0,\mathrm{y};\mathrm{q}) = 0 \quad \hat{\mathrm{f}}'(+\infty,\mathrm{y};\mathrm{q}) = 0 \tag{42}$$

$$\hat{\theta}(0,\mathrm{y};\mathrm{q}) = 1 \quad \hat{\theta}(+\infty,\mathrm{y};\mathrm{q}) = 0 \tag{43}$$

The solution of the zeroth-order deformation equations and their respective boundary conditions for special cases of the embedding parameter q = 0 and q = 1 are given by:

$$\hat{\mathrm{f}}(\mathrm{x},\mathrm{y};0) = \mathrm{f}_0(\mathrm{x},\mathrm{y}) \quad \hat{\theta}(\mathrm{x},\mathrm{y};0) = \theta_0(\mathrm{x},\mathrm{y}) \tag{44}$$
when $\mathrm{q} = 0$

$$\hat{\mathrm{f}}(\mathrm{x},\mathrm{y};1) = \mathrm{f}(\mathrm{x},\mathrm{y}) \quad \hat{\theta}(\mathrm{x},\mathrm{y};1) = \theta(\mathrm{x},\mathrm{y}) \tag{45}$$
when $\mathrm{q} = 1$

Therefore, as q increases from 0 to 1, $\hat{\mathrm{f}}(\mathrm{x},\mathrm{y};\mathrm{q})$ and $\hat{\theta}(\mathrm{x},\mathrm{y};\mathrm{q})$ deform from the initial approximations f_0 and θ_0 to the functions f and θ which are the solutions of Eqs. (15) and (16).

Using Eq. (44), the Taylor series expansions of $\hat{\mathrm{f}}(\mathrm{x},\mathrm{y};\mathrm{q})$ and $\hat{\theta}(\mathrm{x},\mathrm{y};\mathrm{q})$ with respect to the embedding parameter q about q = 0 are written as

$$\hat{\mathrm{f}}(\mathrm{x},\mathrm{y};\mathrm{q}) = \mathrm{f}_0(\mathrm{x},\mathrm{y}) + \sum_{\mathrm{m}=1}^{\infty} \mathrm{f}_\mathrm{m}(\mathrm{x},\mathrm{y})\mathrm{q}^\mathrm{m} \tag{46}$$

$$\hat{\theta}(\mathrm{x},\mathrm{y};\mathrm{q}) = \theta_0(\mathrm{x},\mathrm{y}) + \sum_{\mathrm{m}=1}^{\infty} \theta_\mathrm{m}(\mathrm{x},\mathrm{y})\mathrm{q}^\mathrm{m} \tag{47}$$

where

$$\mathrm{f}_\mathrm{k}(\mathrm{x},\mathrm{y}) = \frac{1}{\mathrm{m}!} \frac{\partial^\mathrm{m} \hat{\mathrm{f}}(\mathrm{x},\mathrm{y};\mathrm{q})}{\partial \mathrm{q}^\mathrm{m}}\bigg|_{\mathrm{q}=0} \tag{48}$$

$$\theta_\mathrm{k}(\mathrm{x},\mathrm{y}) = \frac{1}{\mathrm{m}!} \frac{\partial^\mathrm{m} \hat{\mathrm{f}}(\mathrm{x},\mathrm{y};\mathrm{q})}{\partial \mathrm{q}^\mathrm{m}}\bigg|_{\mathrm{q}=0}$$

Suppose that the spatial-scale parameter λ, the auxiliary parameters $\hbar_f$ and $\hbar_\theta$, and the auxiliary functions H_f (η) and H_θ (η) are properly specified so that the above Taylor series are convergent at q = 1, then setting q = 1 in Eqs. (46) and (47), and employing Eq. (45) yield the following relations for nth-order approximations:

$$f(x,y) \approx f_0(x,y) + \sum_{m=1}^{n} f_m(x,y) \quad (49)$$

$$\theta(x,y) \approx \theta_0(x,y) + \sum_{m=1}^{n} \theta_m(x,y) \quad (50)$$

The next step in the HAM is to obtain $f_m(\eta)$ and $\theta_m(\eta)$ for m = 1, 2, …, n to be used in the mth-order approximations (49) and (50). To this end, the following vectors are defined:

$$\vec{f}_n = \{f_0(x,y), f_1(x,y), f_2(x,y), ..., f_n(x,y)\} \quad (51)$$

$$\vec{\theta}_n = \{\theta_0(x,y), \theta_1(x,y), \theta_2(x,y), ..., \theta_n(x,y)\} \quad (52)$$

Subsequently, the zeroth-order deformation equations (Eqs. (40) and (41)) are differentiated m times with respect to q, and divided by m!. Setting q = 0 in the resulting expressions yield the following mth-order deformation equations for $m \geq 1$:

$$\mathcal{L}_1\left[f_m(x,y) - \chi_m f_{m-1}(x,y)\right] = \hbar_f H_f(x,y)\mathcal{R}_m^f\left[\vec{f}_{m-1}, \vec{\theta}_{m-1}\right] \quad (53)$$

$$\mathcal{L}_2\left[\theta_m(x,y) - \chi_m \theta_{m-1}(x,y)\right] = \hbar_\theta H_\theta(x,y)\mathcal{R}_m^\theta\left[\vec{f}_{m-1}, \vec{\theta}_{m-1}\right] \quad (54)$$

where

$$\chi_m = \begin{cases} 0 & m \leq 1 \\ 1 & m > 1 \end{cases} \quad (55)$$

And

$$\mathcal{R}_m^f\left[\vec{f}_{m-1}, \vec{\theta}_{m-1}\right] = A_1 f'''_{m-1}(x,y) - A_2 \frac{\sin x}{x}\theta_{m-1}(x,y) + \frac{1}{Pr}\left\{\sum_{j=0}^{m-1} f_j(x,y) f'_{m-1-j}(x,y) - \sum_{j=0}^{m-1} f_j(x,y) f''_{m-1-j}(x,y) + y\left[\sum_{j=0}^{m-1} f'_j(x,y)\frac{f'_{m-1-j}(x,y)}{\partial y} - \sum_{j=0}^{m-1}\frac{\partial f_j(x,y)}{\partial y} f''_{m-1-j}(x,y)\right]\right\} \quad (56)$$

$$\mathcal{R}_m^\theta\left[\vec{f}_{m-1}, \vec{\theta}_{m-1}\right] = A_3\theta''_{m-1}(x,y) - \sum_{j=0}^{m-1} f_j(x,y)\theta'_{m-1-j}(x,y) - y\left[\sum_{j=0}^{m-1} f'_j(x,y)\frac{\partial \theta_{m-1-j}}{\partial y} - \sum_{j=0}^{m-1}\theta'_j(x,y)\frac{\partial f_{m-1-j}(x,y)}{\partial y}\right] \quad (57)$$

The boundary conditions for Eqs. (56) and (57) are given by

$$f_m(0,y) = f'_m(0,y) = f'_m(+\infty,y) = \theta_m(0,y) = \theta_m(+\infty,y) = 0 \quad (58)$$

Considering conditions (36) and (37), the solutions of the mth-order deformation, equations can be written in following general forms:

$$f_m(x,y) = \chi_m f_{m-1}(x,y) + \hbar_f \mathcal{L}_1^{-1}\left\{H_f(x,y)\mathcal{R}_m^f\left[\vec{f}_{m-1}, \vec{\theta}_{m-1}\right]\right\} + d_1 + d_2\exp(-\lambda x) + d_3 \quad (59)$$

$$\theta_m(x,y) = \chi_m \theta_{m-1}(x,y) + \hbar_\theta \mathcal{L}_2^{-1}\left\{H_\theta(x,y)\mathcal{R}_m^\theta\left[\vec{f}_{m-1}, \vec{\theta}_{m-1}\right]\right\} + + d_4\exp(-\lambda x) + d_5 \quad (60)$$

Where $\mathcal{L}_1^{-1}$ and $\mathcal{L}_2^{-1}$ denote the inverse of the linear operators $\mathcal{L}_1$ and $\mathcal{L}_2$, respectively, and d_i (i = 1,2,…,5) are integration constants to be determined through the boundary conditions (58).

Since the *high-order deformation equations* are linear and uncoupled, in principle, they can be solved recursively starting from m = 1 up to any desired order by means of a symbolic computation software such as Mathematica required that the auxiliary functions H_f (η) and H_θ (η) are specified. Conforming to the rules of solution expression (Eqs. (30) and (31)), the following auxiliary functions are employed in the present analysis:

$$H_f(x) = H_0(x) = \exp(-\lambda x) \quad (61)$$

CONVERGENCE OF THE HAM AND VALIDATION

As it is observed from the solution procedure of the previous section, there are three auxiliary parameters, namely, $\hbar_f$, $\hbar_\theta$, and λ, which have to be specified to make the HAM solution applicable Liao [45]. In general, for a given Prandtl number and the nanoparticles volume fraction, the effects of the auxiliary parameters λ, $\hbar_f$, and $\hbar_\theta$ on the convergence of the series solution are investigated,

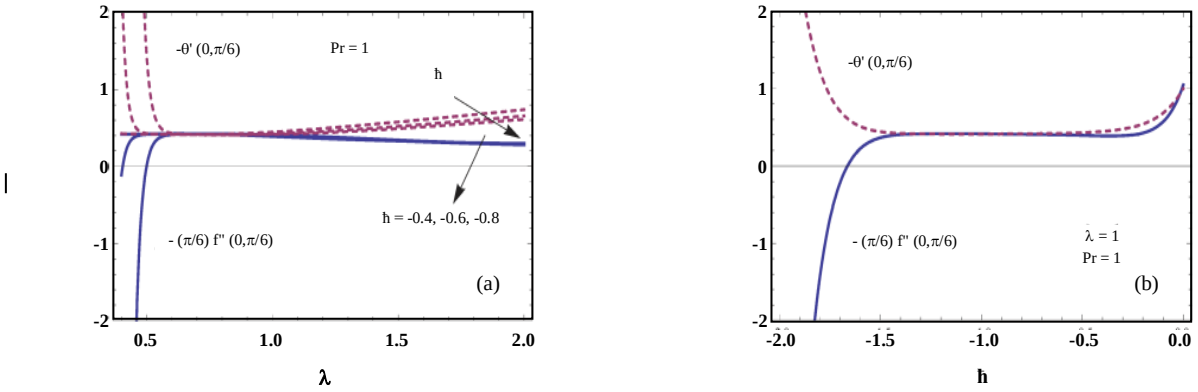

Fig. 4: Effects of λ and ħ on the 12th-order OHAM approximations for Pr = 1: (a) λ-curve; (b) ħ-curve ratio.

and based on the obtained results proper values of the parameters are selected. $f''(0,y)$ and $\theta'(0,y)$ are related to the skin friction and thermal flux at the cylinder surface, respectively. Hence, the effects of the auxiliary parameters on the convergence of $f''(0,y)$ and $\theta'(0,y)$ are examined here.

Figure 4(a) shows the variations of $f''(0,y)$ and $\theta'(0,y)$ with respect to λ for Pr = 1 and $y = \pi/6$, and for three different values of $\hbar$, namely, -0.4, -0.6, and -0.8, using 12th-order series approximations. As can be seen from this figure, $f''(0, \pi/6)$ and $\theta'(0, \pi/6)$ both converge for λ = 0.8. Using the same series approximations as in Fig. 4 and for λ = 0.8, it is observed from Fig. 4(b) that $f''(0,\pi/6)$ and $\theta'(0,\pi/6)$ are convergent for $-0.8 \le \hbar \le -1.3$. Note that the admissible range of $\hbar$ for convergence is the region for which $\hbar$-curves are horizontal. Each value of $\hbar$ belonging to this region yields a converged solution but with a different rate of convergence [45].

OHAM framework

As far as the admissible range of the auxiliary parameters for the nanofluids is concerned, a procedure similar to the one used for Pr = 1 should be conducted for the nanofluids with various nanoparticles volume fractions. In fact, the interval for the admissible values of $\hbar$ varies as the nanoparticles volume fraction, Prandtl number, and nanofluid models change. Theoretically, at the mth-order of approximation, the exact form of square residual errors can defined as

$$\Delta_{i,m} = \int_0^{+\infty}\int \left(N_i\left[\sum_{j=0}^{m} f_j, \sum_{j=0}^{m} \theta_j\right]\right) dxdy, \quad i = 1,2 \qquad (62)$$

It should be noted that $\Delta_{i,m}$ holds at most three unknown convergence-control parameters λ, $\hbar_f$, and $\hbar_\theta$ regardless of the order of approximation. Evidently, more quick reduction in $\Delta_{i,m}$ to zero, expedites the convergence of the corresponding homotopy-series solution. Thus, in practice, at a given order of approximation m, the corresponding optimal values of the three mentioned convergence-control parameters, namely, λ, $\hbar_f$, and $\hbar_\theta$ can be obtained by the minimizing of $\Delta_{i,m}$, corresponding to the following set of three nonlinear algebraic equations

$$\frac{\partial \Delta_{i,m}}{\partial \hbar_f}, \quad \frac{\partial \Delta_{i,m}}{\partial \hbar_\theta}, \quad \frac{\partial \Delta_{i,m}}{\partial \lambda} \qquad (63)$$

Unfortunately, the calculation procedure of the exact square residual error $\Delta_{i,m}$ established by Eq. (62) consumes too much CPU even at low-order of approximations, and thus, is often unfavorable. To overcome this flaw, Liao [55] introduced a more efficient definition of the residual error to replace Eq. (62). Thus, achieving a substantially reduced in the CPU time, the so-called averaged residual error is employed as follows:

$$E_{i,m} = \frac{1}{K}\sum_{s=0}^{K}\left(N_i\left[\sum_{j=0}^{m} f_j(s\Delta x, s\Delta y), \sum_{j=0}^{m} \theta_j(s\Delta x, s\Delta y)\right]\right)^2 \qquad (64)$$

i=1,2

Where $\Delta x = 10/K$, $\Delta y = 10/K$, and K = 20 for the present problem. The above expression for the averaged residual error may grant good enough approximation of the optimal convergence-control parameters. Moreover, the CPU time span for calculating the averaged residual error, $E_{i,m}$ is much less than that of the exact residual error $\Delta_{i,m}$ (Fig. 5). The optimal values of λ and $\hbar$ for three

Table 3: Optimal values of ħ and λ for different values of ϕ using 12th-order series approximations

	Al_2O_3-Water (Model I)		Al_2O_3-Water (Model II)	
ϕ	$\hbar_f = \hbar_\theta = \hbar$	λ	$\hbar_f = \hbar_\theta = \hbar$	λ
0.00	- 0.50	0.60	- 0.50	0.60
0.05	- 0.405	0.57	- 0.412	0.52
0.10	- 0.484	0.53	- 0.365	0.475

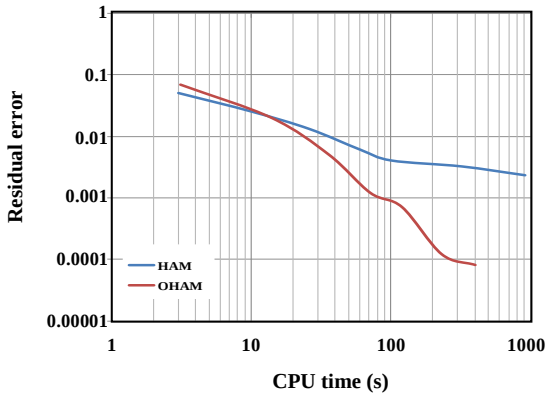

Fig. 5: Comparison of Residual Error versus CPU time (seconds) for HAM and OHAM approaches.

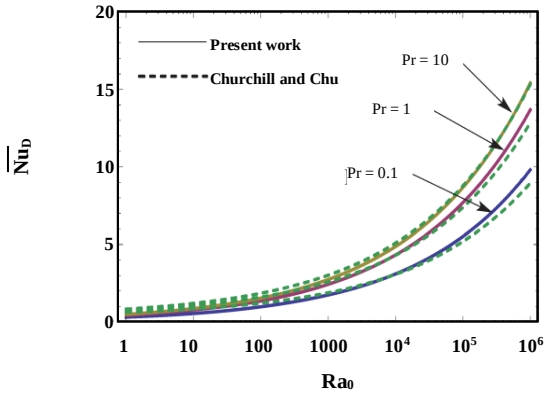

Fig. 6: Comparisons between present 14th-order OHAM solutions with the experimental results of Churchill and Chu [56] for different Prandtl numbers.

different values of the volume fractions of the Al_2O_3 nanoparticles (Models I and II) at 12th-order series approximations are presented in Table 3.

Validation

In order to validate the solution procedure, the natural convection boundary-layer flow and heat transfer along a heated horizontal circular cylinder immersed in a cold fluid is solved using the proposed OHAM for three Prandtl numbers, namely, 0.1, 1 and 10. The obtained results for the average heat transfer coefficient from the cylinder ($\overline{Nu}_D$) are compared with the experimental results of Churchill and Chu [56] for a range of Ra_D from 10 to 10^6. Here, $\overline{Nu}_D$ and Ra_D are the average Nusselt number and the Rayleigh number defined based on the diameter of the cylinder, respectively. As Fig. 6 depicts, very good agreements exist between the experimental results and the 14th-order OHAM series solutions of the average Nusselt number from the cylinder for the entire range of the considered Rayleigh numbers.

Using air (Pr = 0.71) as the working medium, Table 4 shows a comparison between $\overline{Nu}_D$ obtained by the present homotopy analysis with the existing semi-analytical, numerical, and experimental results in the literature for a range of Rayleigh numbers between 10 and 10^8. As it can be observed from the table, very good agreements exist between the present results and the results of the other research work for the entire range of the considered Rayleigh numbers.

RESULTS AND DISCUSSION

Having explored the convergence characteristics of the proposed OHAM, and compared the results obtained by its application to the two test cases with those available in the literature, the OHAM is utilized to investigate the buoyancy-driven flow and heat transfer characteristics along the heated horizontal circular cylinder immersed in Al_2O_3-water nanofluid shown in Fig. 1. The Brinkman formula and *Maïga et al.*'s correlation are employed for the effective viscosity of Al_2O_3-water nanofluid. The results are presented for three volume fractions of the nanoparticles, namely, 0.0 (the base fluid), 0.05, and 0.1.

Figs. 7(a) and (b) show the vertical velocity component and the dimensionless temperature with

Table 4: Comparisons of the present results for $\overline{Nu}_D$ with those of other researchers for free convection from a heated horizontal cylinder immersed in air (Pr = 0.71).

		Value of Ra_D (= $g\beta(T_w-T_\infty)D^3/(\nu\alpha)$)							
Reference	Method	10	10^2	10^3	10^4	10^5	10^6	10^7	10^8
Present work	OHAM	0.769	1.368	2.43	4.32	7.69	13.6	24.3	43.2
Davis [57]	EXP	–	–	2.64	4.7	8.36	14.9	–	–
Koch [58]	EXP	–	–	–	4.12	7.33	13.7	–	–
Senftleben [59]	CLM	1.21	1.64	2.74	4.87	8.66	15.4	27.4	48.7
Merk and Prins [60]	NSE	–	–	–	4.36	7.76	13.8	24.5	43.6
Muntasser and Mulligan [61]	LNS	–	–	–	4.3	7.64	13.6	24.2	43
Clemes et al. [62]	EXP	–	2.03	2.99	4.74	7.85	13.3	23.3	–

CLM: conduction layer model; EXP: experimental; OHAM: optimal homotopy analysis method; LNS: local non-similarity solution; and NSE: numerical solution.

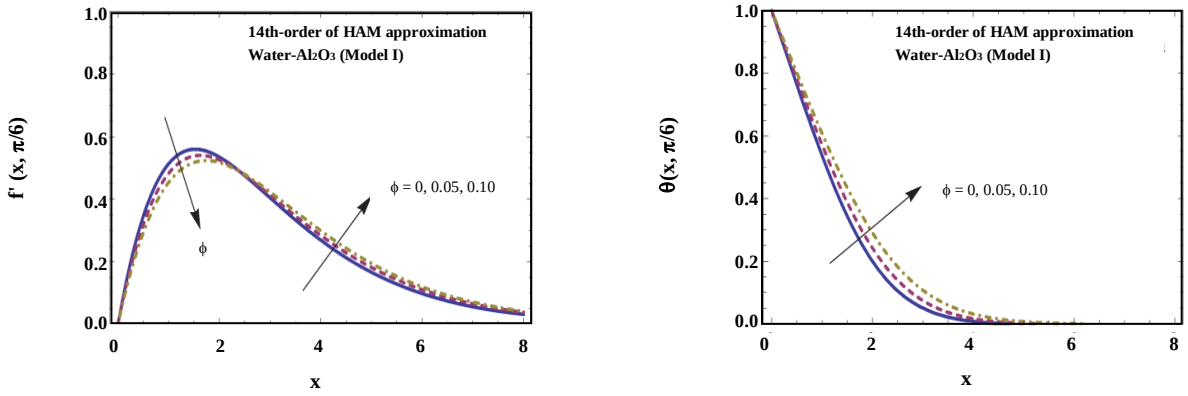

Fig. 7: 14th-order OHAM solutions at $y = \pi/6$ using "Model I" for viscosity: (a) vertical velocity profiles; (b) temperature profiles.

respect to the horizontal local coordinate x, and at $y = \pi/6$ for Al_2O_3-water nanofluid with different volume fractions of nanoparticles, respectively. The Brinkman model for the viscosity of the nanofluid, and 14th-order OHAM approximations has been employed in this case. As it can be observed in Fig. 7(b), for high Prandtl numbers, a heated layer exists next to the wall where the temperature drops from T_w to T_∞. This layer is ruled by the buoyancy ~ friction balance. The vertical velocity component increases from zero at the wall to its peak close to the outer boundary of the heated layer (Fig. 7(a)). Outside this layer, the buoyancy is absent, and the nanofluid is dragged along viscously by the heated layer and restrained its own inertia. Hence, for high Prandtl numbers, the velocity decays to zero in a so-called the velocity boundary layer which is thicker than the thermal layer (Fig. 7(a)).

As far as the nanoparticles volume fraction, the thickness of the heated layer increases with increasing the volume fraction of the nanoparticles (Figs. 7(a) and (b)). The scale analysis shows that, for high Prandtl numbers, the order of the ratio of heated layer thickness for the nanofluid to that of the base fluid is $\left(\overline{\delta}_T/\delta_T\right) \square \left(\overline{Ra}_a/Ra_a\right)^{-1/4}$. As Fig. 3(a) shows, this ratio enlarges with increasing the nanoparticles volume fraction of the Al_2O_3-water nanofluid (Model I) yielding thicker thermal layers with increasing ϕ (Figs. 10(a) and (b)). The order of the ratio of the velocity boundary layer thickness of the nanofluid to that of the base fluid is $\left(\overline{\delta}/\delta\right) \square \left(\overline{Pr}/Pr\right)^{1/2}\left(\overline{Ra}_a/Ra_a\right)^{-1/4}$. Even though, the Prandtl number for the Al_2O_3-water nanofluid (Model I)

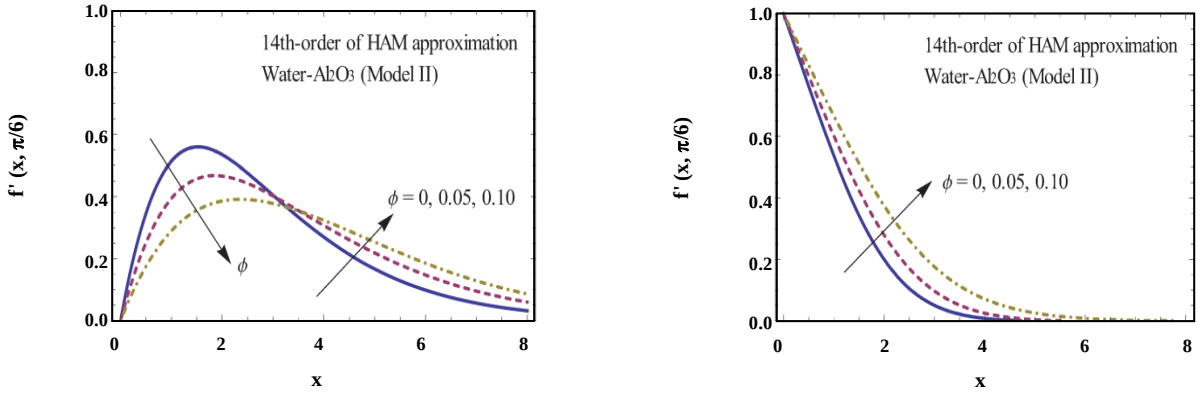

Fig. 8: 14th-order OHAM solutions at y = π/6 using "Model II" for viscosity: (a) vertical velocity profiles; (b) temperature profiles.

decreases mildly with enhancing the volume fraction of the nanoparticles (Fig. 3(b)), the right-hand-side of this relation still increases marginally with increasing the nanoparticles volume fraction. Hence, as Fig. 7(a) shows, the vertical velocity component tends to zero at larger values of x with increasing the volume fraction of the nanoparticles. It is also observed from Fig. 7(a) that the peak and the gradients of the vertical velocity component decrease with increasing the nanoparticles volume fraction. As ϕ increases, the Rayleigh number of the nanofluid decreases while its viscosity increases. Therefore, in the heated layer adjacent to the wall which is ruled by the buoyancy ~ friction balance, both the peak and the gradients of the vertical velocity component decrease as the buoyancy decreases and the nanofluid becomes more viscous.

Figs. 8(a) and (b) show the vertical velocity component and the dimensionless temperature with respect to the horizontal local coordinate x for the Al_2O_3-water nanofluid with different nanoparticles volume fractions, respectively. The Maïga's correlation for the effective viscosity of the nanofluid and 14th-order OHAM approximations has been employed in this case. It is observed from these figures that, similar to the results shown in Figs. 7(a) and (b), the thicknesses of the thermal and velocity boundary layers increase with increasing the volume fraction of the nanoparticles. However, compared to the results of Figs. 7(a) and (b), the increases of $\bar{\delta}_T$ and $\bar{\delta}$ are more in this case. The reductions of the peak and the gradients of the vertical velocity component with increasing ϕ are also more significant compared to what is shown in Fig. 7(a) (Fig. 8(a)). These behaviors are due to the fact that, in Maïga's correlation for the effective viscosity of the alumina-water nanofluid, $\left(\overline{\mathrm{Ra}}_a/\mathrm{Ra}_a\right)^{-1/4}$ and $\left(\overline{\mathrm{Pr}}/\mathrm{Pr}\right)^{1/2}$ are both increasing functions of the nanoparticle volume fraction (Figs. 3(a) and (b)). Moreover, the Al_2O_3-water nanofluid viscosity as obtained by the Maïga's model (Model II) is generally higher than that predicted by the Brinkman model for the entire range of the considered nanoparticles volume fractions. Hence, in this case, with increasing the nanoparticles volume fraction, $\bar{\delta}_T$ and $\bar{\delta}$ increase more, and the peak of the vertical velocity component decreases more compared to the results presented in Fig. 7.

Figs. 9(a) and (b) show the effect of variations of the nanoparticles volume fractions on streamline and the isotherms around the heated cylinder ($0 \le x \le 2\pi$ and $0 \le y \le \pi$) for the Al_2O_3-water nanofluid, respectively. The Brinkman model for the viscosity of the nanofluid (Model I), and 12th-order OHAM approximations are employed in this case. It can be seen from Fig. 9(a) that the maximum value of the stream function decreases and the streamlines become less dense with increasing the volume fraction of the nanoparticles. This is attributed to the fact that the viscosity of the nanofluid is an increasing function of the nanoparticles volume fraction. In addition, as Fig. 9(b) shown, with increasing ϕ, the isotherms get further apart, and the thermal boundary layer thickness rises as $\left(\bar{\delta}_T/\delta_T\right) \propto \left(\overline{\mathrm{Ra}}_a/\mathrm{Ra}_a\right)^{-1/4}$ is an increasing function of the nanoparticles volume fraction (Fig. 3(a)).

Figs. 10 (a) and (b) shows the streamline and isotherms around the heated cylinder in a domain of ($0 \le x \le 2\pi$ and

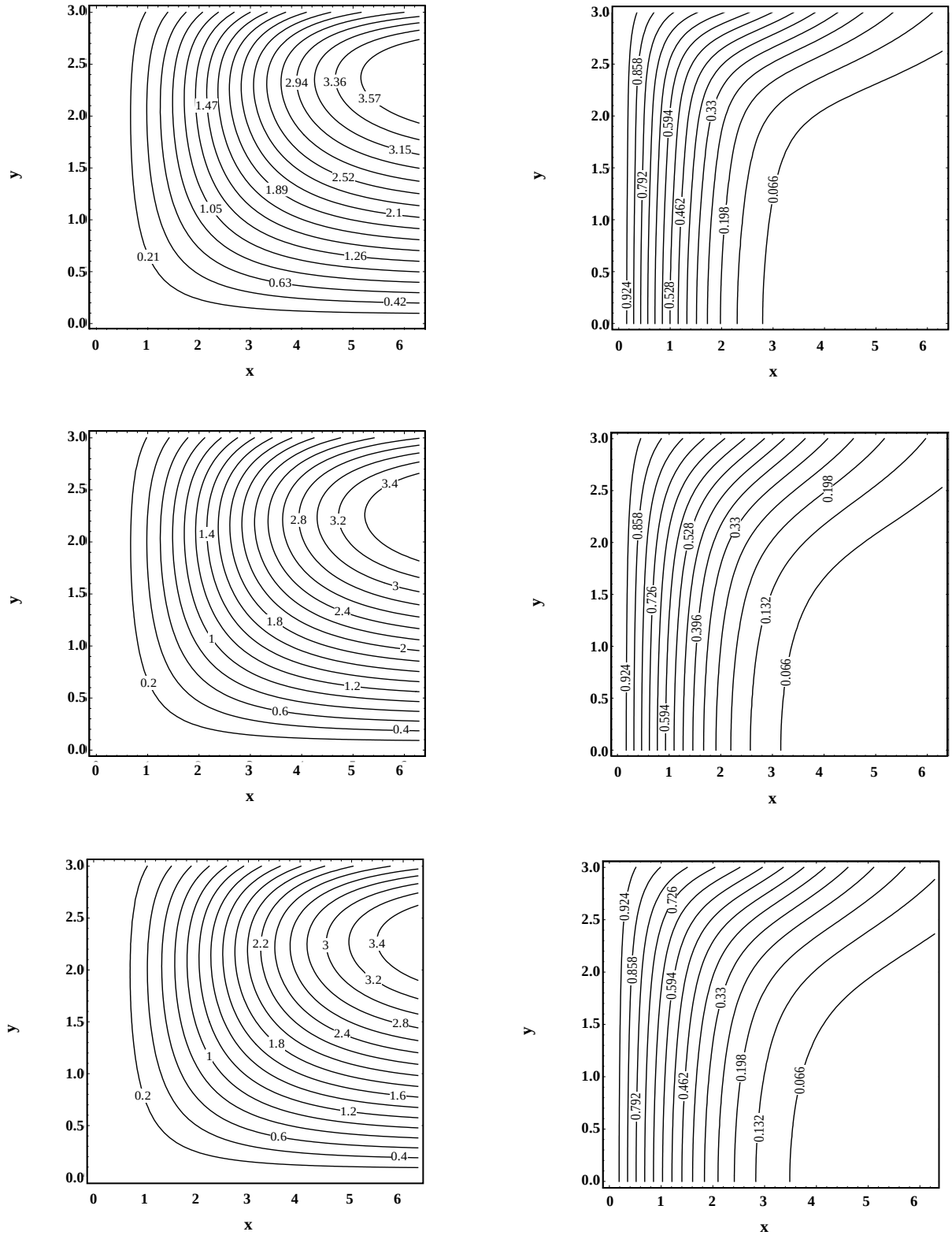

Fig. 9: Streamlines and isotherms for the viscosity of nanofluid (Model I) at 12th-order OHAM series solutions: (a) Streamlines; (b) isotherms.

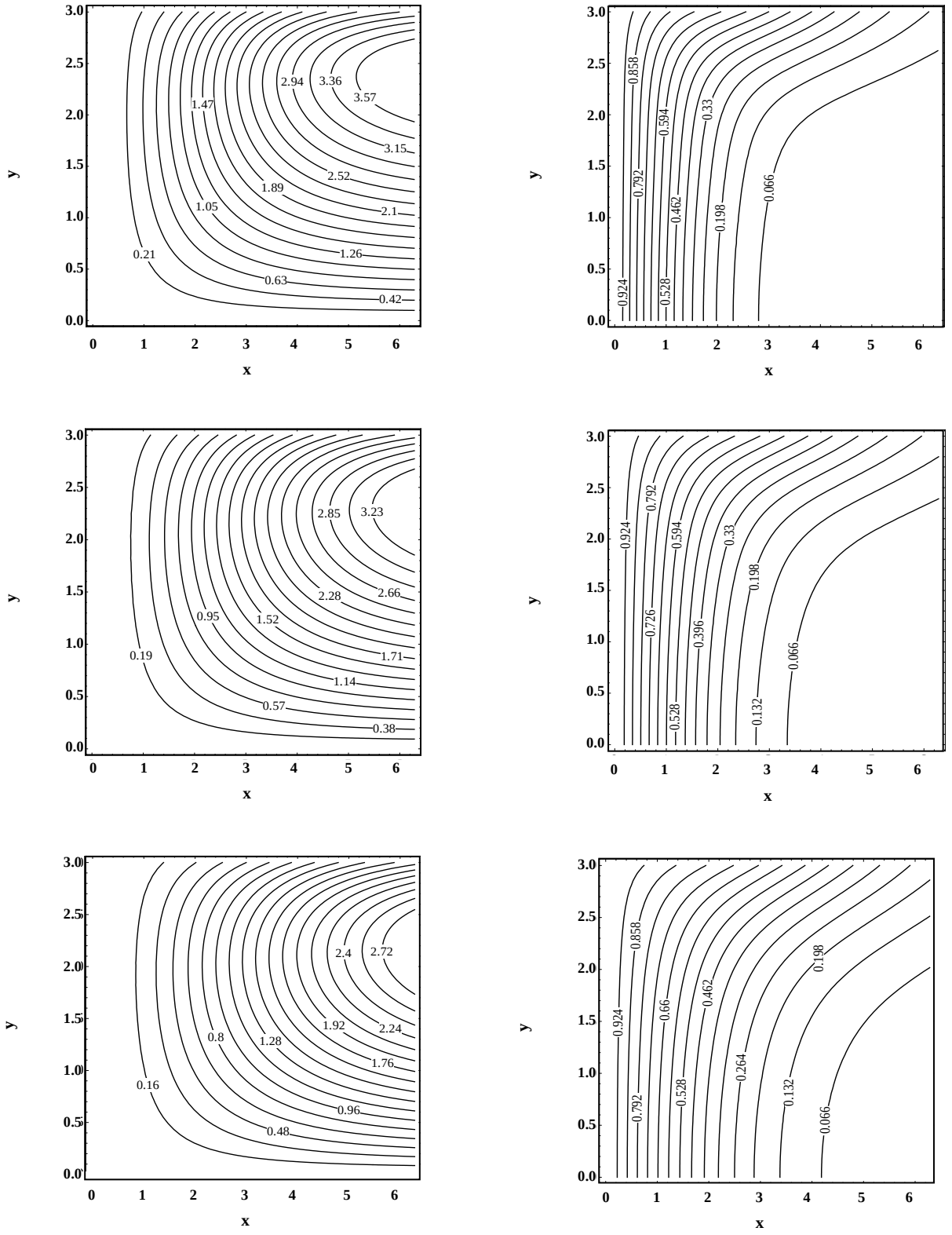

Fig. 10: Streamlines and isotherms for the viscosity of nanofluid (Model II) at 12th-order OHAM series solutions: (a) Streamlines; (b) isotherms

$0 \le y \le \pi$), for the Al_2O_3-water nanofluid with different volume fractions of nanoparticles, respectively. The nanofluid effective viscosity via Maïga's correlation (Model I) and 12th-order OHAM approximations have been employed in this case. It is observed from these figures that, similar to the results shown in Figs. 9(a) and (b), the values of the stream function field decrease and the isotherms become less compact with increasing the nanoparticles volume fraction. However, compared to the results of Figs. 9(a) and (b), $\overline{\delta}_T$ and $\overline{\delta}$ increase more in this case. Besides, the reductions of the stream-function values and the gradients of the temperature field with increasing ϕ are more significant compared to those of Figs. 9(a) and (b) as the viscosity of the Al_2O_3-water nanofluid as attained by the Maïga's correlation is generally higher than that predicted by the Brinkman model for the entire range of the considered nanoparticles volume fractions.

Figs. 11(a) and (b) show the analytical results for the local skin-friction coefficient (Eq. (32)) and the local Nusselt number $Nu_a\, Ra_a^{-1/4}$ of the cylinder for different values of volume fractions of the Al_2O_3-nanoparticles, respectively. The Brinkman viscosity model, and 12th-order OHAM approximations have been employed in this case. Regardless of the magnitude of the nanoparticles volume fraction, it is observed from Fig. 11(a) that the highest heat transfer rate occurs at the lower stagnation point of the circular cylinder ($y \approx 0.0$), and by moving along the periphery of the cylinder toward the upper stagnation point ($y \approx \pi$), the Nusselt number gradually decreases. The skin-friction coefficient initially increases by moving from the lower stagnation point to the maximum value at y approximately equal to $2\pi/3$, and then decreases toward the top of the cylinder (Fig. 11(b)).

As far as the effects of the volume fraction of nanoparticles, it is observed from Fig. 11 that, in general, both the local skin-friction coefficient and the local Nusselt number increase with increasing of ϕ. The increase in the shear stress is due to the fact that the viscosity of the nanofluid is generally an increasing function of the volume fraction. Moreover, the enhancement of the local heat transfer coefficient can be attributed to the fact that the increase of the thermal conductivity of the nanofluid with the volume fraction of the nanoparticles compensates the effect of the reduction of the buoyancy force which tends to decrease with an increase in the nanoparticles volume fraction.

Employing the Maïga's viscosity correlation for the Al_2O_3-nanofluid (Model II), the 12th-order OHAM approximate solutions for the local skin-friction coefficient and the local Nusselt number with respect to y for different values of the volume fractions of the nanoparticles ϕ, are presented in Figs. 12(a) and (b), respectively. The results show similar trends to those of Figs. 11(a) and (b) except that the local heat transfer coefficient is a decreasing function of the nanofluids volume fraction (Fig. 12(b)). The reason being that the decreasing of the inertia with increasing the nanoparticles volume fraction seems to overcome the thermal conductivity enhancement when the Maïga's correlation is employed to model the nanofluid viscosity. Moreover, it is observed from Fig. 12(b) that the increase of the local skin-friction coefficient with increasing the volume fraction of the nanoparticles is more significant compared to that of Fig. 11(b).

The variations of the average Nusselt number defined based on the diameter of the cylinder $\overline{Nu}_D$ with the volume fraction of the nanoparticles for the Al_2O_3-water nanofluid (Model I and II) are presented in Fig. 13. The results are obtained using the 14th-order OHAM approximations. For the Al_2O_3-water nanofluid (Model I), the temperature gradients at the cylinder surface decrease and the heated layer enlarge with increasing the nanoparticles volume fraction (Fig. 7(b)). However, the enhancement of the thermal conductivity of the nanofluids with the nanoparticles volume fraction is large enough to render the average Nusselt number an increasing function of ϕ. For the alumina-water nanofluid (Model II), the temperature gradients at the wall decrease significantly with increasing the volume fraction parameter ϕ (Fig. 8(b)). Hence, as Fig. 13 exhibits, with increasing the nanoparticles volume fraction, the average Nusselt number decreases in this case. However, it should be noted that, basically, there are uncertainties correspond to the nanofluids viscosity behavior. Generally, this is due to the different experimental conditions and setups, as well as various flow regimes which definitely affect the resulting correlations. Many researchers are still working on this issue.

Based on the above results, the following correlations are proposed for the average Nusselt numbers of the nanofluid in terms of the diametrical-based Rayleigh number and the volume fraction of the nanoparticles:

$$\overline{\mathrm{Nu}}_D = \left(0.4667 + 0.1213\phi^{0.6817}\right)\mathrm{Ra}_D^{1/4} \qquad (65)$$

for (Model I)

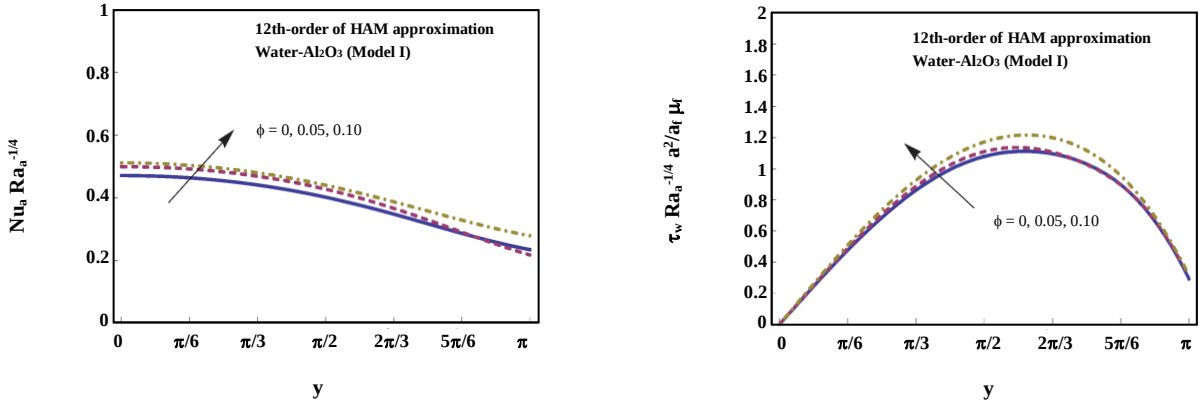

Fig. 11: Local Nusselt number and skin friction coefficient versus ϕ using "Model I": (a) local Nusselt number; (b) skin-friction coefficient.

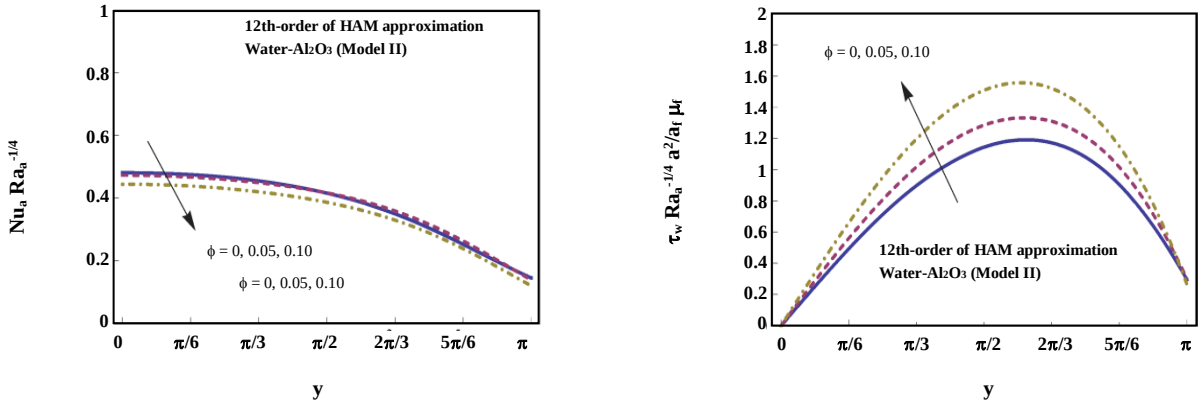

Fig. 12: Local Nusselt number and skin friction coefficient versus ϕ using "Model II": (a) local Nusselt number; (b) skin-friction coefficient.

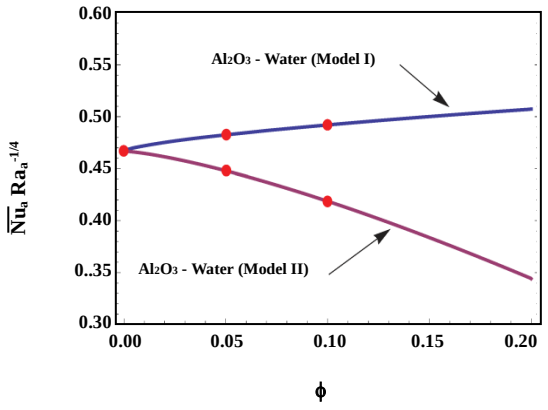

Fig. 13: Variations of the average Nusselt number with the volume fraction of the nanoparticles (Solid lines: correlated curves; red spot: calculated via OHAM).

$$\overline{Nu}_D = \left(0.4667 - 1.0761\phi^{1.35014}\right) Ra_D^{1/4} \quad (65)$$

for (Model II)

CONCLUSIONS

The uncertainties of viscosity on buoyancy-driven fluid flow and heat transfer along a horizontal heated circular cylinder immersed in a cold Al_2O_3-water nanofluid is investigated via the Optimal Homotopy Analysis Method (OHAM). The validity of the solution procedure is demonstrated through the consenting results of the OHAM and the experimental and numerical solutions. The analytical solutions for the velocity and temperature fields obtained through the application of the OHAM to the above free convection, the problem is more flexible and efficient

compared to the existing results in the literature. Moreover, choosing the optimal values for the auxiliary parameters through the convergence study guarantees a superior control on the convergence and accuracy of the solutions via OHAM framework.

The results of the performed parametric study reveal that the average Nusselt number is accurately predicted for various Prandtl and Rayleigh numbers, and different working mediums such air and water. Moreover, it is concluded from the results that the enhancement or suppression of the heat transfer from the circular cylinder with increasing the volume fraction of the nanoparticles strongly depends on the viscosity model used for the nanofluid. Based on the results of the parametric study, different correlations are proposed for the average Nusselt number of the nanofluid in terms of the Rayleigh number ($10 \leq Ra \leq 10^6$), and the nanoparticles volume fraction ($0.0 \leq \phi \leq 0.10$). The results of this study show that the OHAM is a promising analytical technique for solving highly nonlinear fluid flow and heat transfer problems.

NOMENCLATURE

a	Radius of the circular cylinder, m
c_p	Specific heat at constant-pressure, J/kg.K
D	Tube diameter, m
f	Dimensionless stream function
g	Gravitational acceleration, m/s^2
h	Heat transfer coefficient, W/m^2 K
k	Thermal conductivity, W/m.K
Nu	Local Nusselt number
$\overline{Nu}$	Average Nusselt number
Pr	Prandtl number, ν/a
q"	Surface heat flux, W/m^2
Ra	Rayleigh number, $g\beta\Delta Ta^3/(\nu\alpha)$
T	Temperature, K
u,v	Dimensionless velocities in (x,y) directions
x,y	Dimensionless coordinates

Greeks

α	Thermal diffusivity, $k/\rho c_p$, m^2/s
β	Thermal expansion coefficient, K^{-1}
δ	Velocity boundary layer thickness, m
δ_T	Thermal boundary layer thickness, m
θ	Dimensionless temperature function
μ	Dynamic viscosity, Pa s
ν	Kinematic viscosity, m^2/s
ρ	Density, kg/m^3
τ_w	Wall shear stress, Pa
ϕ	Volume fraction of nanoparticles
ψ	Stream function

Subscripts

D	Diameter
f	Base fluid, water
nf	Nanofluid
p	Particle
w	Tube wall
∞	Ambient

Superscripts

^	Dimensional
–	Nanofluid

Received : Jun. 18, 2017 ; Accepted : Jan. 15, 2018

REFERENCES

[1] Sparrow E.M., Lee L., Analysis of Mixed Convection About a Circular Cylinder, *International Journal of Heat Mass Transfer*, **19**: 229–236 (1976).

[2] Merkin J.H., Free Convection Boundary Layer on an Isothermal Horizontal Circular Cylinder, *ASME/AIChE, Heat Transfer Conference*, St. Louis, MO (1976).

[3] Merkin J.H., Free Convection Boundary Layers on Cylinders of Elliptic Cross Section, *Journal of Heat Transfer*, **99**(3): 453-457 (1977).

[4] Merkin J.H., Mixed Convection a Horizontal Circular Cylinder, *International Journal of Heat and Mass Transfer*, **20**: 73–77 (1977).

[5] Ingham D.B., Free-Convection Boundary Layer on an Isothermal Horizontal Cylinder, *Journal of Applied Mathematics and Physics (ZAMP)*, **29**(6):871-883 (1978).

[6] Kuehn T.H., Goldstein R.J., Numerical Solution to the Navier-Stokes Equations for Laminar Natural Convection About a Horizontal Isothermal Circular Cylinder, *International Journal of Heat and Mass Transfer*, **23**(7): 971-979 (1980).

[7] Merkin J.H., Pop I., A Note on the Free Convection Boundary Layer on a Horizontal Circular Cylinder with Constant Heat Flux, *Wärme- und Stoffübertragung*, **22**(1-2):79-81 (1988).

[8] Morgan V.T., Heat Transfer by Natural Convection from a Horizontal Isothermal Circular Cylinder in Air, *Heat Transfer Engineering*, **18**(1):25-33 (1997).

[9] Nazar R., Amin N., Pop I., Free Convection Boundary Layer on a Horizontal Circular Cylinder with Constant Heat Flux in a Micropolar Fluid, *International Journal of Applied Mechanics and Engineering*, **7**(2):409–431 (2002).

[10] Molla M.M., Hossain M.A., Gorla R., Natural Convection Flow from an Isothermal Horizontal Circular Cylinder with Temperature Dependent Viscosity, *Heat and Mass Transfer*, **41**(7): 594-598 (2005).

[11] Molla M.M., Hossain M.A., Paul M.C., Natural Convection Flow from an Isothermal Horizontal Circular Cylinder in Presence of Heat Generation, *International Journal of Engineering Science*, **44**(13–14): 949-958 (2006).

[12] Molla M.M., Paul S.C., Hossain M.A., Natural Convection Flow from a Horizontal Circular Cylinder with Uniform Heat Flux in Presence of Heat Generation, *Applied Mathematical Modelling*, **33**(7): 3226-3236 (2009).

[13] Chung B.-J., Eoh J.-H., Heo J.-H., Visualization of Natural Convection Heat Transfer on Horizontal Cylinders, *Heat and Mass Transfer*, **47**(11):1445-1452 (2011).

[14] Prhashanna A., Chhabra R.P., Laminar Natural Convection from a Horizontal Cylinder in Power-Law Fluids, *Industrial & Engineering Chemistry Research*, **50**(4): 2424-2440 (2011).

[15] Azim N.A., Chowdhury M.K., MHD-Conjugate Free Convection from an Isothermal Horizontal Circular Cylinder with Joule Heating and Heat Generation, *Journal of Computational Methods in Physics*, **2013**:11 (2013).

[16] Bhuiyan A., Azim N., Chowdhury M., Joule Heating Effects on MHD Natural Convection Flows in Presence of Pressure Stress Work and Viscous Dissipation from a Horizontal Circular Cylinder, *Journal of Applied Fluid Mechanics*, **7**(1):7-13 (2014).

[17] Javed T., Majeed A., Mustafa I., MHD Effects on Natural Convection Laminar Flow from a Horizontal Circular Cylinder in Presence of Radiation, *Revista Mexicana de Física*, **61**:450-457 (2015).

[18] Sebastian G., Shine S.R., Natural Convection from Horizontal Heated Cylinder with and Without Horizontal Confinement, *International Journal of Heat and Mass Transfer*, **82**:325-334 (2015).

[19] Das S.K., Choi S.U.S., Yu W., Pradeep T., "Nanofluids: Science and Technology", John Wiley & Sons, Inc., pp. 389-397 (2007).

[20] Wang X.-Q., Mujumdar A.S., Heat Transfer Characteristics of Nanofluids: a Review, *International Journal of Thermal Sciences*, **46**(1):1-19 (2007).

[21] Wang X.-Q., Mujumdar A.S., A Review on Nanofluids - Part I: Theoretical and Numerical Investigations, *Brazilian Journal of Chemical Engineering*, (2008).

[22] Kakaç S., Pramuanjaroenkij A., Review of Convective Heat Transfer Enhancement with Nanofluids, *International Journal of Heat and Mass Transfer*, **52**(13–14):3187-3196 (2009).

[23] Arefmanesh A., Amini M., Mahmoodi M., Najafi M., Buoyancy-Driven Heat Transfer Analysis in Two-Square Duct Annuli Filled with a Nanofluid, *European Journal of Mechanics - B/Fluids*, **33**: 95-104 (2012).

[24] Bég O.A., Rashidi M.M., Akbari M., Hosseini A., Comparative Numerical Study of Single-Phase and Two-Phase Models for Bio-Nanofluid Transport Phenomena, *Journal of Mechanics in Medicine and Biology*, **14**(01): 1450011 (2014).

[25] Goodarzi M., Safaei M.R., Vafai K., Ahmadi G., Dahari M., Kazi S.N., Jomhari N., Investigation of Nanofluid Mixed Convection in a Shallow Cavity Using a Two-Phase Mixture Model, *International Journal of Thermal Sciences*, **75** (Supplement C): 204-220 (2014).

[26] Jani S., Mahmoodi M., Amini M., Akbari M., Free Convection in Rectangular Enclosures Containing Nanofluid with Nanoparticles of Various Diameters, **45**(2): 145-169 (2014).

[27] Jafari A., Shahmohammadi A., Mousavi S.M., CFD Investigation of Gravitational Sedimentation Effect on Heat Transfer of a Nano-Ferrofluid, *Iranian Journal of Chemistry and Chemical Engineering (IJCCE)*, **34**(1): 87-96 (2015).

[28] Khalili S., Tamim H., Khalili A., Rashidi M.M., Unsteady Convective Heat and Mass Transfer in Pseudoplastic Nanofluid over a Stretching Wall, *Adv. Powder Technol.*, **26**(5):1319-1326 (2015).

[29] Kherbeet A.S., Mohammed H.A., Salman B.H., Ahmed H.E., Alawi O.A., Rashidi M.M., Experimental Study of Nanofluid Flow and Heat Transfer over Microscale Backward- and Forward-Facing Steps, *Exp. Therm Fluid Sci.*, **65** (Supplement C): 13-21 (2015).

[30] Mohebbi K., Rafee R., Talebi F., Effects of Rib Shapes on Heat Transfer Characteristics of Turbulent Flow of Al2O3-Water Nanofluid inside Ribbed Tubes, *Iranian Journal of Chemistry and Chemical Engineering (IJCCE)*, **34**(3): 61-77 (2015).

[31] Bashirnezhad K., Bazri S., Safaei M.R., Goodarzi M., Dahari M., Mahian O., Dalkılıça A.S., Wongwises S., Viscosity of Nanofluids: A Review of Recent Experimental Studies, *International Communications in Heat and Mass Transfer*, **73**(Supplement C):114-123 (2016).

[32] Bhatti M.M., Rashidi M.M., Effects of Thermo-Diffusion and Thermal Radiation on Williamson Nanofluid over a Porous Shrinking/Stretching Sheet, *J. Mol. Liq.*, **221**(Supplement C):567-573 (2016).

[33] Rashidi M.M., Nasiri M., Khezerloo M., Laraqi N., Numerical Investigation of Magnetic Field Effect on Mixed Convection Heat Transfer of Nanofluid in a Channel with Sinusoidal Walls, *Journal of Magnetism and Magnetic Materials*, **401** (Supplement C): 159-168 (2016).

[34] Safaei M., Ahmadi G., Goodarzi M., Kamyar A., Kazi S., Boundary Layer Flow and Heat Transfer of FMWCNT/Water Nanofluids over a Flat Plate, *Fluids*, **1**(4):31 (2016).

[35] Safaei M., Ahmadi G., Goodarzi M., Safdari Shadloo M., Goshayeshi H., Dahari M., Heat Transfer and Pressure Drop in Fully Developed Turbulent Flows of Graphene Nanoplatelets–Silver/Water Nanofluids, *Fluids*, **1**(3):20 (2016).

[36] Safaei M.R., Shadloo M.S., Goodarzi M.S., Hadjadj A., Goshayeshi H.R., Afrand M., Kazi S.N., A Survey on Experimental and Numerical Studies of Convection Heat Transfer of Nanofluids Inside Closed Conduits, *Advances in Mechanical Engineering*, **8**(10):1687814016673569 (2016).

[37] Akram S., Nadeem S., Influence of Nanoparticles Phenomena on the Peristaltic Flow of Pseudoplastic Fluid in an Inclined Asymmetric Channel with Different Wave Forms, *Iranian Journal of Chemistry and Chemical Engineering (IJCCE)*, **36**(2):107-124 (2017).

[38] Arani A.A.A., Akbari O.A., Safaei M.R., Marzban A., Alrashed A.A.A.A., Ahmadi G.R., Nguyen T.K., Heat Transfer Improvement of Water/Single-Wall Carbon Nanotubes (SWCNT) Nanofluid in a Novel Design of a Truncated Double-Layered Microchannel Heat Sink, *International Journal of Heat and Mass Transfer*, **113**(Supplement C):780-795 (2017).

[39] Valipour M.S., Ghadi A.Z., Numerical Investigation of Fluid Flow and Heat Transfer Around a Solid Circular Cylinder Utilizing Nanofluid, *International Communications in Heat and Mass Transfer*, **38**(9): 1296-1304 (2011).

[40] Nazar R., Tham L., Pop I., Ingham D.B., Mixed Convection Boundary Layer Flow from a Horizontal Circular Cylinder Embedded in a Porous Medium Filled with a Nanofluid, *Transp Porous Med*, **86**(2): 517-536 (2011).

[41] Tham L., Nazar R., Pop I., Mixed Convection Boundary Layer Flow Past a Horizontal Circular Cylinder Embedded in a Porous Medium Saturated by a Nanofluid: Brinkman Model, *Journal of Porous Media*, **16**(5): 445-457 (2013).

[42] Prasad V.R., Gaffar S.A., Reddy E.K., Bég O.A., Flow and Heat Transfer of Jeffreys Non-Newtonian Fluid from Horizontal Circular Cylinder, *Journal of Thermophysics and Heat Transfer*, **28**(4):764-770 (2014).

[43] Prasad V.R., Gaffar S.A., Bég O.A., Heat and Mass Transfer of Nanofluid from Horizontal Cylinder to Micropolar Fluid, *Journal of Thermophysics and Heat Transfer*, **29**(1):127-139 (2014).

[44] Reddy P.S., Chamkha A.J., Heat and Mass Transfer Characteristics of Nanofluid over Horizontal Circular Cylinder, *Ain Shams Engineering Journal*, (2016).

[45] Liao S., "Beyond Perturbation: Introduction to the Homotopy Analysis Method". Chapman and Hall/CRC (2003).

[46] Brinkman H.C., The Viscosity of Concentrated Suspensions and Solutions, *The Journal of Chemical Physics*, **20**(4):571-571 (1952).

[47] Maïga S.E.B., Palm S.J., Nguyen C.T., Roy G., Galanis N., Heat Transfer Enhancement by Using Nanofluids in Forced Convection Flows, *International Journal of Heat and Fluid Flow*, **26**(4):530-546 (2005).

[48] Batchelor G.K., The effect of Brownian motion on the Bulk Stress in a Suspension of Spherical Particles, *J. Fluid Mech.*, **83**(1):97-117 (2006).

[49] Corcione M., Empirical Correlating Equations for Predicting the Effective Thermal Conductivity and Dynamic Viscosity of Nanofluids, *Energy Convers. Manage.*, **52**(1):789-793 (2011).

[50] Heyhat M.M., Kowsary F., Rashidi A.M., Momenpour M.H., Amrollahi A., Experimental Investigation of Laminar Convective Heat Transfer and Pressure Drop of Water-Based Al_2O_3 Nanofluids in Fully Developed Flow Regime, *Exp. Therm Fluid Sci.*, **44**(Supplement C):483-489 (2013).

[51] Chandrasekar M., Suresh S., Chandra Bose A., Experimental Investigations and Theoretical Determination of Thermal Conductivity and Viscosity of Al_2O_3/Water Nanofluid, *Exp. Therm Fluid Sci.*, **34**(2):210-216 (2010).

[52] Sekhar Y.R., Sharma K.V., Study of Viscosity and Specific Heat Capacity Characteristics of Water-Based Al_2O_3 Nanofluids at Low particle Concentrations, *Journal of Experimental Nanoscience*, **10**(2):86-102 (2015).

[53] Hatschek E., The General Theory of Viscosity of Two-Phase Systems, *Transactions of the Faraday Society*, **9**(0): 80-92 (1913).

[54] Garnett J.C.M., Colours in Metal Glasses and in Metallic Films, *Philosophical Transactions of the Royal Society of London A: Mathematical, Physical and Engineering Sciences*, **203**(359-371): 385-420 (1904).

[55] Liao S., An Optimal Homotopy-Analysis Approach for Strongly Nonlinear Differential Equations, *Communications in Nonlinear Science and Numerical Simulation*, **15**(8):2003-2016 (2010).

[56] Churchill S.W., Chu H.H.S., Correlating Equations for Laminar and Turbulent Free Convection from a Horizontal Cylinder, *International Journal of Heat and Mass Transfer*, **18**(9):1049-1053 (1975).

[57] Davis A.H., XXXI. Natural Convective Cooling of Wires, *Philosophical Magazine Series 6*, **43**(254): 329-339 (1922).

[58] Koch W., Über die Wärmeabgabe Geheizter Rohre Bei Verschiedener Neigung der Rohrachse, *Gesundh. Ing. Beih.*, **22**(1):1–29 (1927).

[59] Senftleben H., DieWärmeabgabe von Körpern verschiedener Form in Flüssigkeiten und Gasen Bei Freier Strömung, *Zeitschrift für Angewandte Physik*, **3**:361-373 (1951).

[60] Merk H.J., Prins J.A., Thermal Convection in Laminar Boundary Layers III, *Appl. sci. Res.*, **4**(3): 207-221 (1954).

[61] Muntasser M.A., Mulligan J.C., A Local Nonsimilarity Analysis of Free Convection from a Horizontal Cylindrical Surface, *Journal of Heat Transfer*, **100**(1): 165-167 (1978).

[62] Clemes S.B., Hollands K.G.T., Brunger A.P., Natural Convection Heat Transfer from Long Horizontal Isothermal Cylinders, *Journal of Heat Transfer*, **116**(1): 96-104 (1994).